ACS Catalysis

Research Article

pubs.acs.org/acscatalysis

Catalytic Reactions on the Open-Edge Sites of Nitrogen-Doped Carbon Nanotubes as Cathode Catalyst for Hydrogen Fuel Cells

Feng Gao,[†] Guang-Lin Zhao,*[,†] and Shizhong Yang[‡]

[†]Department of Physics and Nano Catalysts Laboratory, Southern University and A&M College, Baton Rouge, Louisiana 70813 United States

[‡]Department of Computer Science, Southern University and A&M College, Baton Rouge, Louisiana 70813 United States

Supporting Information

ABSTRACT: Recent experimental reports proposed that pyridinic-type sites on the open edges of carbon nanotubes (CNTs) may contribute to the high catalytic activity for oxygen reduction reaction (ORR) on nitrogen-doped CNTs (N-CNTs). Herein, we performed first-principles spin-polarized density functional theory calculations to examine the catalytic steps for ORR and water formation reaction (WFR) on the open edges of N-CNTs. For half-N doping on the open edge of CNTs (HN-CNTs), O_2 and OOH can be chemisorbed and partially reduced on the C−N bridge site without an energy barrier. The subsequent WFR for reduced O_2/OOH with ambient H^+ and additional electrons can be finished without energy barrier for the formation of two H_2O molecules. The second H_2O molecule needs an energy of ∼0.49 eV to be desorbed from the catalytic site, which completes an electrocatalytic reaction cycle on the cathode catalyst for hydrogen fuel cells (HFCs). For H-saturated open-edge sites of HN-CNT, ORR and WFR can also be completed energetically. For full-N doping on the open edge of CNTs (FN-CNTs), O_2 can be reduced and dissociated on the N−N bridge site with an energy barrier of 0.81 eV during the ORR. The WFR steps can then be finished spontaneously. OOH can also be adsorbed and reduced on the N−N bridge site of FN-CNTs, and the subsequent WFR steps can be completed spontaneously. The rate-limiting steps for the full electrocatalytic reactions on N-CNTs as cathode catalyst for HFCs are determined.

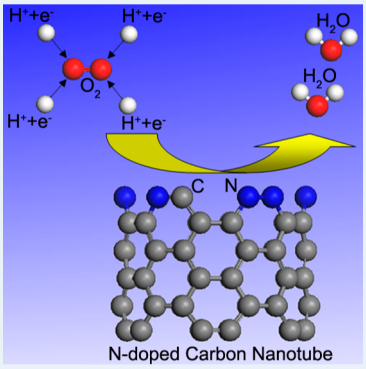

KEYWORDS: *first-principles calculations, electrocatalytic reactions, nitrogen-doped carbon nanotubes, cathode catalyst, fuel cells*

1. INTRODUCTION

In the past several years, several research groups have reported that nitrogen-doped carbon nanotubes (N-CNTs) can be used as new cathode catalysts for the oxygen reduction reaction (ORR) for hydrogen fuel cells (HFCs).[1−9] Liu et al. at Argonne Nationaql Laboratory prepared vertically aligned carbon nanotubes (ACNT) using a versatile chemical vapor deposition method and demonstrated that ACNTs functionalized through nitrogen and iron doping can be electrocatalytically active for ORR.[3] Dai and co-workers reported that vertically aligned nitrogen-containing carbon nanotubes can act as a metal-free electrode with a much better electrocatalytic activity, long-term operation stability, and tolerance to crossover effect than platinum for oxygen reduction in alkaline fuel cells.[4] Although there are a large number of reports on the high ORR activities of N-CNTs, the full electrocatalytic reactions on N-CNTs as a metal-free cathode catalyst for HFCs remains unclear. It has been proposed that N-CNTs catalyze the ORR process on the cathode of HFCs through a four-electron pathway.[4,8] The high ORR electrocatalytic activity of N-CNTs was ascribed to the high degree of edge exposure or the great number of pyridinic-type nitrogen sites.[4,7,8,10] To understand the electrocatalytic reaction steps on the open edge of N-CNTs, we performed first-principles spin-polarized density functional theory (DFT) calculations for short pieces of single-walled CNTs with nitrogen doping. We calculated the elementary catalytic reaction steps, minimum energy pathways (MEPs) for full catalytic reaction cycles on the open edges of N-CNTs as the cathode catalyst for HFC. These include the ORR and water formation reaction (WFR) processes. We have also calculated the activation energies for the rate-limiting steps in ORR and WFR.

2. COMPUTATIONAL METHODS

The present first-principles spin-polarized DFT calculations were performed by using the Vienna ab initio simulation package (VASP),[11−13] which implemented the projector augmented plane wave[14,15] potentials. The exchange-correlation interaction potentials and energies were described by local density approximation. The dispersion correction was included in the DFT computations by using the DFT-D2 method[16] implemented in VASP. An energy cutoff of 400 eV was employed. In the self-consistent DFT computations, the calculated total energy converged to less than 1×10^{-5} eV. The atomic positions were fully relaxed in all the DFT calculations until the residual forces were less than 0.05 eV/Å on the atoms. A supercell with lattice parameters of 15 Å × 18

Received: October 16, 2013
Published: March 17, 2014

   dx.doi.org/10.1021/cs500221m | ACS Catal. 2014, 4, 1267−1273

Å × 15 Å and $\alpha = \beta = \gamma = 90°$ was used to simulate the N-CNTs and interactions with O_2 and H^+ and additional electrons. According to the experimental reports, the synthesized N-CNTs exhibit a bamboo-like structure, a great part of which consists of open ends of relatively short CNTs.[1,2,4,17−19] Individual short CNTs are weakly stacked one on the top of the other to create a long nanofiber. In this work, short pieces of (6, 6) CNT with 6 carbon atomic rings were used. Our first-principles DFT calculations show that the total energy of the short piece (6, 6) CNT with an N-doping at the open edge is lower than that with an N-doping in its middle wall by 1.93 eV. Therefore, N substitutional doping tends to locate at the open edge of the short CNT. In addition, Ozkan and co-workers studied the role of graphitic edge plane exposure in N-doped carbon nanofibers for ORR.[20] They proposed that edge-N content is the electrocatlytic active site for ORR. Here, we study the possible electrocatalytic reactions on the open edge of the N-CNTs.

Two N doping cases were considered (also see Figure S1 in Supporting Information (SI)): half N-doping on the open edge of short CNTs, in which half of the carbon atoms at the open edge are substituted by N atoms (HN-CNT); and full N-doping on the open edge of short CNTs, in which all the carbon atoms at the open edge are substituted by N atoms (FN-CNT). We focus on the electrocatalytic reaction on the C−N and CH-NH bridge sites of HN-CNT and the N−N bridge site of the FN-CNT. The MEPs of the reaction processes were calculated by using a nudged elastic band (NEB) method[21−23] implemented in VASP. By using this method, we have successfully calculated the MEPs for ORR and WFR on nitrogen-doped fullerenes.[24]

3. RESULTS AND DISCUSSION

3.1. Oxygen Reduction Reaction (ORR) on C−N Bridge Site of HN-CNTs. In this work, we first studied half N-doping on the open edge of short CNTs, in which half of the carbon atoms at the open edge are substituted by N atoms (HN-CNT) (shown in Figure S1 in Supporting Information (SI)). We calculated the effective charges and charge transfers for the system by Bader charge analysis using the code developed by Henkelman et al.[25] At the open edge, the calculated charge transfers (CT) for N and C atoms are $N^{-2.94}$ and $C^{+1.67}$, respectively. N-Doping also induced magnetism to the open edge of the CNT. The calculated magnetic moments are 0.15 μ_B/N and 0.49 μ_B/C, respectively. Figure 1a shows the relative potential energy for ORR on the C−N bridge site of HN-CNT. The embedded images in Figure 1a show the side views of relaxed atomic structures for the initial, intermediate, transition, and final states. The corresponding top views are shown in Figure S2 in the SI.

In the initial state, an O_2 molecule is far away from the C−N bridge site, with O−C and O−N distances at 3.0 Å. After O_2 adsorption (the intermediate state), the O_2 molecule is partially reduced on the C−N bridge site of the short CNT. The O−O bond length is increased to 1.45 Å from the O−O bond length (1.22 Å) of free O_2 molecule. The O(1)−C and O(2)−N bond lengths are 1.36 and 1.49 Å, respectively. Here, O(1) refers to the oxygen atom bonded to a carbon atom, and O(2) refers to the O atom atop the nitrogen atom at the C−N bridge site. The O(1)−C bond is much stronger than the O(2)−N bond. The calculated charge transfers for the two O atoms are $O(1)^{-0.92}$ and $O(2)^{-0.18}$, respectively. An additional quantity to describe the ORR is the change of the magnetic moment of O_2

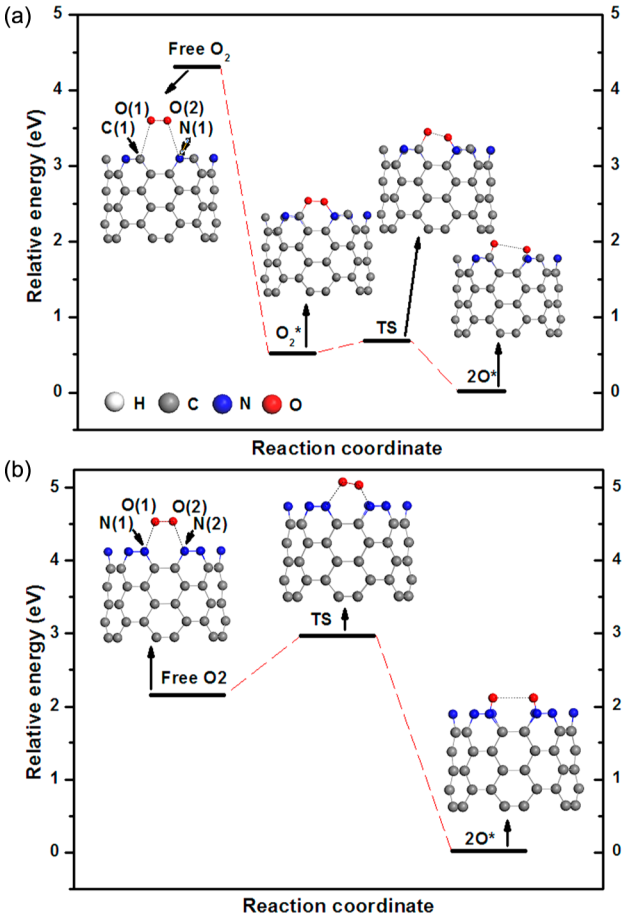

Figure 1. Relative potential energies for ORR on (a) C−N bridge site of HN-CNT and (b) N−N bridge site of FN-CNT.

molecule. The magnetic moment of the reduced O_2 is 0.01 μ_B. In comparison, a free O_2 molecule has a magnetic moment of 2.0 μ_B. There is no activation energy barrier for this O_2 adsorption and partial reduction process. The partially reduced O_2 needs to overcome an activation energy barrier of 0.15 eV, crossing a transition state (TS) (which has a maximum total energy among the nearby reaction configurations), and becomes much dissociated (the final state).

We further calculated the vibrational frequencies of the two O atoms at the TS. In the harmonic approximation, the calculated vibrational frequencies of the two O atoms are 995, 590, 405, 323, 231, and 85i cm^{-1}, respectively. There is only one imaginary frequency, which is related to the vibration of the reduced O_2 along the MEP. The result confirmed that the TS derived from the NEB calculation is a saddle point. At the TS, the O−O bond length is 1.67 Å; the O(1)−C and O(2)−N bond lengths are 1.44 and 1.26 Å, respectively. Charge transfers for the two O atoms at the TS are $O(1)^{-0.95}$ and $O(2)^{-0.32}$, respectively. The magnetic moment of the reduced O_2 is 0.065 μ_B.

In the final state, the partially reduced O_2 is further dissociated after crossing an energy barrier of 0.15 eV; the O−O distance is 2.74 Å; and the O(1)−C and O(2)−N bond lengths become 1.22 and 1.26 Å, respectively. The calculated charge transfers for the two O atoms become $O(1)^{-1.82}$ and $O(2)^{-0.43}$, respectively. The magnetic moment of the reduced O_2 in the final state is 0.0. Figure 2a displays the 3-D iso surfaces (with an iso density value of 0.1 e/Å^3) of the electron

dx.doi.org/10.1021/cs500221m | ACS Catal. 2014, 4, 1267−1273

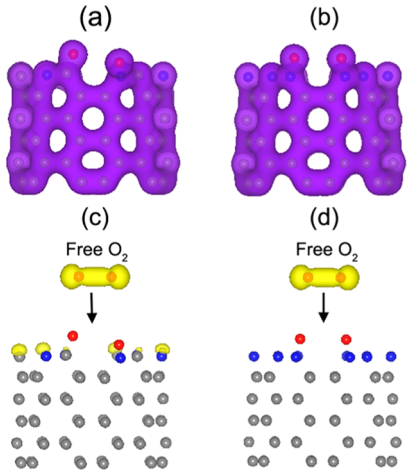

Figure 2. 3-D electron density maps for reduced O_2 on (a) C−N bridge site of HN-CNT and (b) N−N bridge site of FN-CNT; (c, d) 3-D magnetization density maps after ORR on the two catalytic sites.

density (spin-up plus spin-down) map of the reduced O_2 on the C−N bridge site of HN-CNT. Clearly, the electron density in the region between the two O atoms is greatly reduced after O_2 reduction. The overlaps of the electron densities between O(1) and C, as well as O(2) and N, indicate the formations of new O(1)−C and O(2)−N bonds. Figure 2c shows the 3-D iso surfaces (with an iso density value of 0.05 e/Å^3) of magnetization density (which is defined as spin-up density minus spin-down density) map of O_2 before and after reduction on the C−N bridge site of HN-CNT. The magnetization density between the two O atoms is also much reduced after O_2 reduction on the C−N bridge site of the HN-CNT. The calculated magnetic moments of both the reduced O(1) and O(2) are 0 μ_B, much smaller than the magnetic moment of 1.0 μ_B per O atom in free O_2 molecule.

3.2. Water Formation Reaction on C−N Bridge Site of HN-CNTs. As discussed by Kaukonen and co-workers,[26,27] to achieve high catalytic activity toward ORR through nitrogen-relaxed defect at the cathode electrode of HFCs, the activation energies for the ORR and subsequent water formation reaction (WFR) for the reduced O_2 with H^+ and e^- reactions should not be too high. We further performed a series of first-principles spin-polarized DFT calculations to examine the possibilities of the WFR after ORR on the C−N bridge site of HN-CNT. To simulate the four-electron electrocatalytic reaction process at the cathode of HFCs step by step, we introduce one H^+ and one additional electron for each reaction step and then calculate the MEP for the reaction process with the reduced O_2. To simulate the ambient H^+ and additional electrons around the reduced O_2, the initial state of H should be as free as possible. Therefore, in each WFR step, we first introduce one H, which is far away (3.0 Å) from the reduced O_2, O, or OH. For the reaction of H with O_2 or O, H is initially placed 3.0 Å atop O_2/O. For the reaction between H and OH, H is initially positioned with an O−H distance of 3.0 Å and a H−O−H angle of 104.5°, which is the same as the H−O−H angle in a free H_2O molecule. Then the system is fully relaxed by first principles DFT calculations to obtain a stable state for subsequent NEB calculations.

Figure 3a shows the possible electrocatalytic reaction steps for a full electrocatalytic reaction cycle involving ORR and WFR on the C−N bridge site of HN-CNT. Using the relative

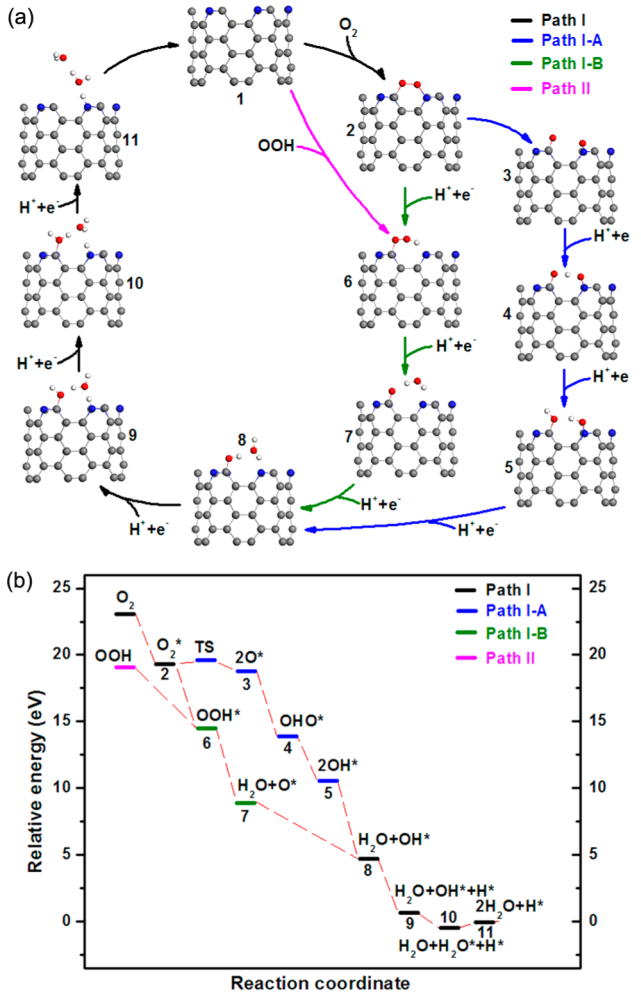

Figure 3. (a) Possible electrocatalytic reaction steps involving ORR and WFR on the C−N bridge site of HN-CNT. (b) Relative potential energy for the MEPs of the electrocatalytic reaction cycles.

potential energy, Goddard et al. studied the oxygen hydration mechanism for the ORR at the Pt and Pd as cathode catalysts for fuel cells.[28] Figure 3b shows the relative potential energies for the MEPs of the possible electrocatalytic reaction cycles on the C−N bridge site of HN-CNT. Detailed structures for the WFR steps are shown in SI Figure S3. To simulate WFR after O_2 reduction and dissociation on the C−N bridge site, we first introduce one free H^+ and an additional electron. The H atom is adsorbed by the reduced O_2, forming a kind of OOH (step 4 of path I-A in Figure 3a). The H atom is bonded to both O(1) and O(2). The O(1)−H and O(2)−H bond lengths are 1.27 and 1.45 Å, respectively. There is no activation energy barrier for the OOH formation reaction (as can be seen from the relative potential energy in Figure 3b).

We then introduced another H^+ and additional electron moving close to the formed OOH (step 5). The second H reacts with O(1), forming an OH adsorbed on C. At the same time, the first H moves closer to O(2), forming another OH adsorbed on N. The O(1)−H and O(2)−H bond lengths are 0.99 Å and 1.0 Å, respectively. There is no activation energy barrier for this OH formation reaction. Subsequently, we introduced a third H^+ and an additional electron to the system. They can react with OH, which is adsorbed on N, forming a H_2O(2) molecule (step 8). The OH bond length and H−O−H bond angle are 1.0 Å and 107.8°, respectively. No activation

dx.doi.org/10.1021/cs500221m | ACS Catal. 2014, 4, 1267−1273

energy is needed for the H_2O formation process. We then introduced the fourth H^+ and additional electron moving close to OH that is adsorbed on C. The relaxed structure is shown in step 9 in Figure 3a). The fourth H could not react with OH on the C site and directly produce a second H_2O molecule ($H_2O(1)$). Instead, it reacts with the O atom, forming an OH. The as-formed $H_2O(2)$ molecule grabs one H from OH and gives one H to N, forming NH (see step 9). During this WFR step, the previously formed OH on C and the $H_2O(2)$ molecule act as a shuttle, which transfers the fourth introduced H^+ and additional electron to the N site. There is no activation energy barrier for this H transferring process.

We then introduced the fifth H^+ and additional electron moving close to OH on C, which forms a $H_2O(1)$ molecule without an activation energy (step 10). The $H_2O(1)$ is bonded to C, with a C−O bond length of 1.44 Å. The OH bond length and H−O−H in $H_2O(1)$ are 1.0 Å and 121.2°, respectively. The O(2)−N distance becomes 3.0 Å. The OH bond length and H−O−H bond angle in $H_2O(2)$ are 0.98 Å and 110.5°, respectively. We also evaluated the desorption process of the $H_2O(1)$ molecule. By overcoming a desorption energy of 0.49 eV, $H_2O(1)$ could be desorbed from the C site (step 11) (O(1)−C bond length is 4.34 Å). After the formations and desorptions of the two water molecules from the C−N bridge site, the HN-CNT recovers back to its original structure, and the full catalytic reaction cycle is completed. The C−N bridge site is ready for the next catalytic reaction cycle.

Our first-principles spin-polarized DFT calculations also show the possibility of O_2 hydration before full reduction on the C−N bridge site of HN-CNT. As shown in path I-B in Figure 3a, one H^+ and additional electron could react with the partially reduced O_2, forming an OOH, which is adsorbed on the C−N bridge site (step 6 in Figure 3a). There is no activation energy barrier for the OOH formation. The O(1)−C bond length is 1.34 Å. The H atom is bonded to reduced O_2, with a bond length of 1.04 Å. The N−H distance is 1.57 Å, which indicates a weak bonding between N and H. Then the second H^+ and additional electron could react with OOH, forming a $H_2O(2)$ (step 7) without an activation energy. The O(2)−N distance is 2.89 Å. The O−H bond length and H−O−H bond angle in $H_2O(2)$ are 0.99 Å and 100.0°, respectively. The O(1)−C bond decreases to 1.23 Å, indicating that O(1) is more strongly grabbed by the carbon atom on the CNT after the formation of $H_2O(2)$. Subsequently, the third H^+ and additional electron react with O(1), forming an OOH that is adsorbed on C (step 8). Path I-B merges with path I-A at step 8 into path I for the rest WFR steps. Comparison of the relative potential energies for paths I-A and I-B indicates that for a full electrocatalytic reaction cycle on the C−N bridge site of HN-CNT, WFR based on partially reduced O_2 is more favorable than that based on fully reduced/dissociated O_2. There is no need for O_2 to be completely reduced to complete the WFR.

We also examined another possible pathway for the first electron transfer process in the electrocatalytic reaction cycle, that is, an ORR starting with OOH adsorption. SI Figure S4 shows the relative potential energy for the OOH adsorption reaction on the C−N bridge site of HN-CNT. Initially, an OOH is far away from the C−N bridge site, where the O−C and O−N distances are 2.96 and 2.95 Å, respectively. The OOH could be adsorbed and reduced on the C−N bridge site without any activation energy (see step 6 of path II in Figure 3). The reduced OOH then proceeds with the WFR steps as discussed above for path I-B. The relative potential energies shown in Figure 3b indicate that a full electrocatalytic reaction cycle starting with OOH adsorption and reduction is quite favorable on the C−N catalytic site of HN-CNT.

It is possible that H atoms could be adsorbed on the edge sites of the CNT before any ORR and WRF. Therefore, we also calculated the electrocatalytic reaction steps on the C−N bridge site of HN-CNT with the edge C and N sites saturated by H atoms (the CH−NH bridge site) (see step 1 in Figure 4a).

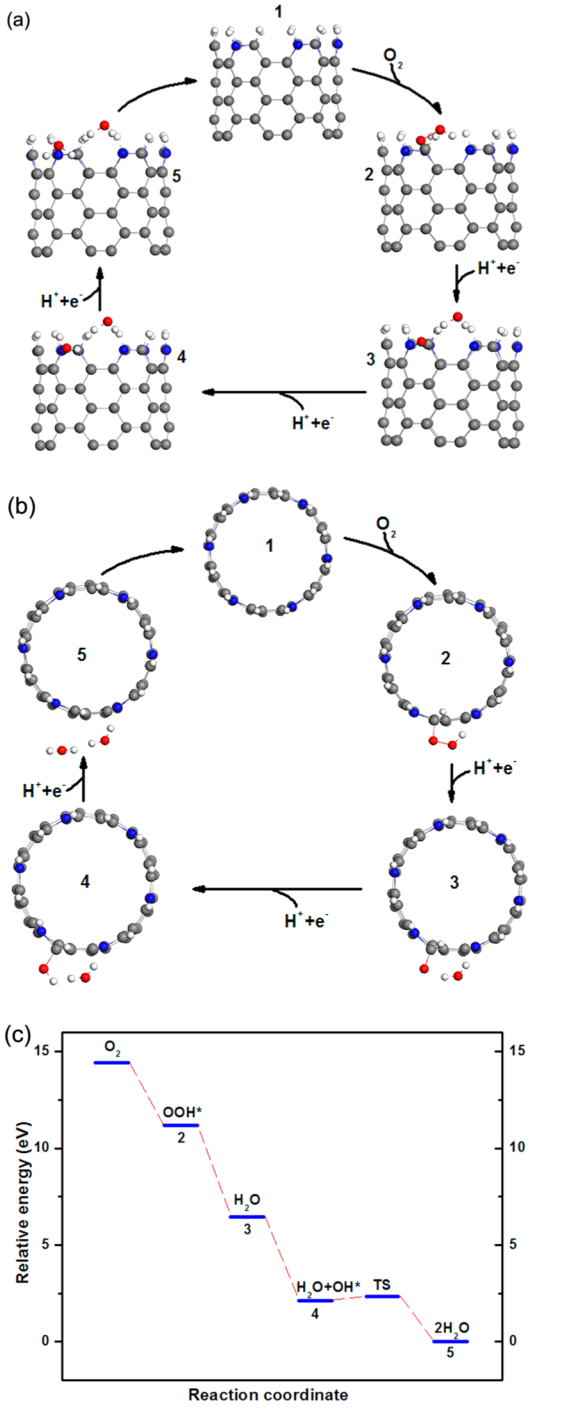

Figure 4. Possible electrocatalytic reaction steps on the CH−NH bridge site of HN-CNT. Embedded are (a) side and (b) top views of relaxed structures for the reaction steps. The relative potential energy for the MEP of the electrocatalytic reaction cycle is presented in part c.

dx.doi.org/10.1021/cs500221m | ACS Catal. 2014, 4, 1267−1273

Figure 4a shows the electrocatalytic reaction steps on the CH−NH bridge site of HN-CNT. Embedded are the side views of the relaxed atomic structures for each reaction step. The electrocatalytic reaction steps related to top views of the atomic structures are shown in Figure 4b. Figure 4c shows the corresponding relative potential energy for the MEP of the electrocatalytic reaction cycle. A free O_2 molecule can be adsorbed and reduced on the CH−NH bridge site by forming a C−O bond (step 2 in Figure 4). The C−O bond length is 1.43 Å. Meanwhile, the H atom on the N site react with O_2, forming an OOH adsorbed on the C site. There is no activation energy barrier for this OOH formation step. A H^+ and an additional electron can react with the OOH without an activation energy, producing a H_2O molecule, which then desorbs away from the catalytic site (step 3). Subsequently, another H^+ and additional electron reacts with the O atom pending on the C site, forming an OH adsorbed on C (step 4). No activation energy is needed for the OH formation step.

Finally, by overcoming an activation energy barrier of 0.19 eV and crossing a TS, a third H^+ and additional electron can react with the OH that is adsorbed on the C site of the CH−NH bridge site, forming the second H_2O molecule and then desorbing from the catalytic site (step 5). The calculated vibrational frequencies of the H^+ in the TS are 734, 389, and 1033i cm^{-1}, respectively. There is only one imaginary frequency along MEP, indicating that the TS derived from NEB calculation is a saddle point. Bader charge analysis shows that after OH reduction, the charge transfer for the O atom is $O^{-1.7}$ which is bonded to C. When a H^+ moves close to OH from a free state to the TS, there is a potential energy reduction of ∼1.49 eV due to the Coulomb electric interaction. Part of the change of potential energy will transfer to the kinetic energy of H^+ in the dynamical process that is not included in the DFT calculation, which was done essentially at $T = 0$ K. The kinetic energy of the H^+, when it reaches the TS, can easily overcome the activation energy barrier (0.19 eV) during the WFR for the formation of the second H_2O molecule. With the formation and desorption of the two H_2O molecules from the CH−NH bridge site, a full catalytic reaction cycle is completed. The HN-CNT recovers back to its original structure and is ready for the next catalytic reaction cycle.

3.3. Oxygen Reduction Reaction on N−N Bridge Site of FN-CNTs. For further comparisons, we also examined the ORR and WFR processes on the N−N bridge site of full N-doping on the open edge of short CNT (FN-CNT). Bader charge analysis for the charge transfer shows that the N atoms at the open edge become $N^{-1.32}$. The C atoms that are bonded to N atoms become $C^{+1.30}$. There is a substantial charge transfer from the C atoms to the N atom around the doping site. The calculated magnetic moment of the N atom is 0.0. The MEP for ORR is shown in Figure 1b. Embedded images show the side views of relaxed atomic structures for the initial, transition, and final states. Detailed side and top views of the initial, transition, and final states are shown in Figure S5 in the SI.

In the initial state, the O−N distances are at 2.67 Å. To move close to the N−N bridge site, O_2 needs to overcome an activation energy barrier of 0.81 eV to cross the TS, and then become much dissociated with an O−O bond length at 2.60 Å. We calculated the vibrational frequencies of O_2 at the TS for the ORR process. In harmonic approximation, the calculated vibrational frequencies of O_2 are 953, 510, 366, 149, 114, and 268i cm^{-1}. There is only one imaginary frequency related to the vibration of O_2 along the MEP. The TS derived from the NEB calculation is a saddle point. At the TS, the O−O bond length is 1.29 Å, which is 0.08 Å larger than the O−O bond length (1.21 Å) in a free O_2. O(1)−N and O(2)−N distances are 1.98 and 1.64 Å, respectively. The calculated charge transfers on the two O atoms are $O(1)^{-0.10}$ and $O(2)^{-0.06}$, respectively. The calculated magnetic moments of O(1) and O(2) are 0.51 μ_B and 0.16 μ_B, respectively. After crossing over the TS, the O_2 molecule becomes much reduced, with an O−O distance of 2.60 Å. The O(1)−N and O(2)−N bond lengths are 1.23 Å. The calculated charge transfers for the two O atoms are $O(1)^{-0.41}$ and $O(2)^{-0.42}$, respectively. The magnetic moment of the reduced O_2 is nearly 0. There is not much covalent bonding electron density between O(1) and O(2) (Figure 2b) because of the reduction and dissociation of the O_2 molecule; however, the overlaps of the electron densities between O(1) and N(1) as well as O(2) and N(2) indicate the formations of new O(1)−N and O(2)−N bonds. The magnetization density in the region between the two O atoms is greatly reduced after O_2 dissociation on the N−N bridge site of the FN-CNT (Figure 2d). The calculated magnetic moments of the dissociated O(1) and O(2) are 0 μ_B.

3.4. Water Formation Reaction on N−N Bridge Site of FN-CNTs. For the purpose of comparisons, we further studied the WFR steps for the reduced O_2 on the N−N bridge site of FN-CNT. Figure 5 shows the electrocatalytic reaction steps and relative potential energies for full electrocatalytic reaction cycles involving ORR and WFR on the N−N bridge site of FN-CNT. More details for the WFR pathways are shown in SI Figure S6. As shown in path I in Figure 5, a H atom can be adsorbed by O(1) and O(2) and trapped between them (step 3 in Figure 5), forming a kind of OOH. The O(1)−H and O(2)−H bonds are 1.24 and 1.17 Å, respectively. The O(1)−N and O(2)−N bond lengths are elongated to 1.30 and 1.31 Å (from 1.23 Å), respectively. There is no activation energy barrier for this step. A second H^+ and electron can react with O(1), forming an OH bonded to N(1) (step 4). Meanwhile, the H adsorbed between the two O atoms moves to O(2), forming an OH bonded to N(2). After the formation of the two OH, the O(1)−N and O(2)−N bond lengths are elongated to 1.38 and 1.35 Å, respectively. There is no activation energy barrier for this reaction step. Subsequently, a third H^+ and additional electron can react with O(2)H, producing a $H_2O(2)$ molecule, which then desorbs from the catalytic site (step 7). The O−H bond length and H−O−H bond angle in $H_2O(2)$ are 0.99 Å and 107.1°, respectively. The formation of $H_2O(2)$ needs no activation energy. Finally, the OH on N(1) can further react with another H^+ and additional electron, and form the second water molecule, $H_2O(1)$, which then desorbs from the adsorption site (step 8). The O(1)−N distance is 2.81 Å. In addition, there is no activation energy barrier for the formation of the second water molecule. The relative potential energy in path I in Figure 4b indicates that as long as the O_2 molecule overcomes an activation energy barrier of 0.81 eV to be reduced and dissociated (ORR step) on the N−N bridge site, the following WFR steps will be very favorable without any activation energy barrier.

Path II in Figure 5 shows the pathway for the electrocatalytic reaction steps starting with OOH adsorption on the N−N site of FN-CNT. The corresponding relative potential energy for OOH adsorption and reduction on the N−N bridge site of FN-CNT is shown in SI Figure S7. Initially, an OOH is about 3.0 Å atop the N−N bridge site. The OOH can be adsorbed and reduced onto the N−N bridge site without any activation

dx.doi.org/10.1021/cs500221m | ACS Catal. 2014, 4, 1267−1273

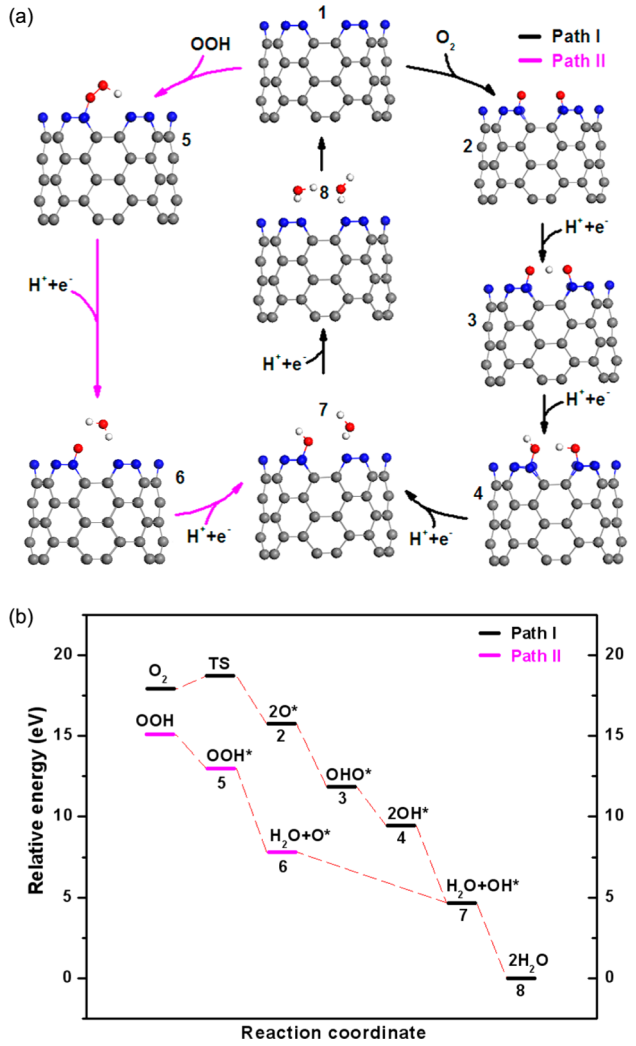

Figure 5. (a) Possible electrocatalytic reaction steps involving ORR and WFR on the N−N bridge site of FN-CNT. (b) Relative potential energies for the MEPs of the electrocatalytic reaction cycles.

barrier by forming an O(1)−N bond in step 5. After reduction, the O(1)−N bond length is 1.36 Å, and the N(2)−H distance is 1.60 Å, indicating the H is weakly bonded to the N(2). The O−O bond length is increased to 1.44 Å from 1.22 Å in a free OOH. A second H^+ and additional electron can react with the adsorbed OOH, forming a H_2O(2) molecule (step 6 in Figure 5). No activation barrier is needed for the formation of H_2O(2). The O(1)−N bond decreases to 1.24 Å from 1.36 Å. Then the third H^+ and additional electron can be adsorbed on N(1) to form an OH without any activation energy (step 7 in Figure 5). The subsequent WFR steps are the same as discussed above for path I. From Figure 5b, we can see that on the N−N bridge site of FN-CNT, the electrocatalytic reaction cycle starting from OOH adsorption is more favorable than that from O_2 dissociation.

4. CONCLUSIONS

In summary, by utilizing first-principles spin-polarized DFT calculations, we studied the full electrocatalytic reaction cycle involving ORR and WFR on open edges of N-CNTs. On the C−N bridge site of HN-CNT, O_2 and OOH can be chemisorbed and partially reduced without an activation energy barrier. The subsequent WFR for the reduced O_2/OOH with ambient H^+ and additional electrons can be completed spontaneously in the formation of two H_2O molecules. The second water molecule needs an energy of about 0.49 eV to be fully desorbed from the catalytic site and complete the electrocatalytic reaction cycle on the cathode catalyst for HFCs. There is no need for the adsorbed O_2 to be fully reduced to complete the WRF cycle. H_2O desorption is the rate-limiting step for the electrocatalytic reaction on the open edge of the HN-CNT catalyst. In the case of a H-saturated open edge of HN-CNT, ORR and WFR can also be completed energetically on the CH−NH site. As comparisons, we also studied the ORR and WFR on the open edge of FN-CNTs. On the N−N bridge site of FN-CNT, O_2 can be reduced and dissociated with an activation energy barrier of 0.81 eV. The following WFR steps can be finished spontaneously without any activation energy barrier. ORR is the rate-limiting step for the electrocatalytic reaction on the open edge of FN-CNT. OOH adsorption, reduction, and the subsequent WFR steps on the N−N bridge site of FN-CNT can also be completed spontaneously. The electrocatalytic reaction cycle starting from OOH adsorption is more favorable than that from O_2 dissociation on the N−N bridge site of FN-CNT.

■ ASSOCIATED CONTENT

Supporting Information

Detailed structures for the model used in the present calculations, and for the reaction steps of ORR and WFR. This material is available free of charge via the Internet at http://pubs.acs.org.

■ AUTHOR INFORMATION

Corresponding Author

*E-mail: Guang-Lin_Zhao@subr.edu.

Notes

The authors declare no competing financial interest.

■ ACKNOWLEDGMENTS

The work was funded in part by the National Science Foundation (NSF) LASIGMA Project (EPS-1003897, NSF92010-15-RII-SUBR), AFOSR (FA9550-09-1-0367), NSF project (CBET-0754821), and support from the U.S. Department of Energy (DE-FE0003693, DE-FE0004734, DE-FE0007220 and DE-FE0008382). All the computations were performed on Louisiana Optical Network Initiative (LONI) computers.

■ REFERENCES

(1) Matter, P.; Ozkan, U. *Catal. Lett.* **2006**, *109*, 115−123.
(2) Matter, P. H.; Zhang, L.; Ozkan, U. S. *J. Catal.* **2006**, *239*, 83−96.
(3) Yang, J.; Liu, D.-J.; Kariuki, N. N.; Chen, L. X. *Chem. Commun.* **2008**, 329−331.
(4) Gong, K.; Du, F.; Xia, Z.; Durstock, M.; Dai, L. *Science* **2009**, *323*, 760−764.
(5) Yang, S.; Zhao, G.-L.; Khosravi, E. *J. Phys. Chem. C* **2010**, *114*, 3371−3375.
(6) Kundu, S.; Nagaiah, T. C.; Xia, W.; Wang, Y.; Dommele, S. V.; Bitter, J. H.; Santa, M.; Grundmeier, G.; Bron, M.; Schuhmann, W.; Muhler, M. *J. Phys. Chem. C* **2009**, *113*, 14302−14310.
(7) Rao, C. V.; Cabrera, C. R.; Ishikawa, Y. *J. Phys. Chem. Lett.* **2010**, *1*, 2622−2627.
(8) Sharifi, T.; Hu, G.; Jia, X.; Wågberg, T. *ACS Nano* **2012**, *6*, 8904−8912.

(9) Tuci, G.; Zafferoni, C.; D'Ambrosio, P.; Caporali, S.; Ceppatelli, M.; Rossin, A.; Tsoufis, T.; Innocenti, M.; Giambastiani, G. *ACS Catal.* **2013**, *3*, 2108−2111.
(10) Matter, P. H.; Wang, E.; Arias, M.; Biddinger, E. J.; Ozkan, U. S. *J. Mol. Catal A: Chem.* **2007**, *264*, 73−81.
(11) Kresse, G.; Hafner, J. *Phys. Rev. B* **1993**, *47*, 558−561.
(12) Kresse, G.; Furthmüller, J. *Comput. Mater. Sci.* **1996**, *6*, 15−50.
(13) Kresse, G.; Furthmüller, J. *Phys. Rev. B* **1996**, *54*, 11169−11186.
(14) Blöchl, P. E. *Phys. Rev. B* **1994**, *50*, 17953−17979.
(15) Kresse, G.; Joubert, D. *Phys. Rev. B* **1999**, *59*, 1758−1775.
(16) Grimme, S. *J. Comput. Chem.* **2004**, *25*, 1463−1473.
(17) Ma, X.; Wang, E.; Zhou, W.; Jefferson, D. A.; Chen, J.; Deng, S.; Xu, N.; Yuan, J. *Appl. Phys. Lett.* **1999**, *75*, 3105−3107.
(18) Ma, X.; Wang, E. G. *Appl. Phys. Lett.* **2001**, *78*, 978−980.
(19) Ma, X.; Wang, E. G.; Tilley, R. D.; Jefferson, D. A.; Zhou, W. *Appl. Phys. Lett.* **2000**, *77*, 4136−4138.
(20) Biddinger, E. J.; Ozkan, U. S. *J. Phys. Chem. C* **2010**, *114*, 15306−15314.
(21) Henkelman, G.; Jonsson, H. *J. Chem. Phys.* **2000**, *113*, 9978−9985.
(22) Henkelman, G.; Uberuaga, B. P.; Jonsson, H. *J. Chem. Phys.* **2000**, *113*, 9901−9904.
(23) Jónsson, H. *Annu. Rev. Phys. Chem.* **2000**, *51*, 623−653.
(24) Gao, F.; Zhao, G.-L.; Yang, S.; Spivey, J. J. *J. Am. Chem. Soc.* **2012**, *135*, 3315−3318.
(25) Sanville, E.; Kenny, S. D.; Smith, R.; Henkelman, G. *J. Comput. Chem.* **2007**, *28*, 899−908.
(26) Kaukonen, M.; Kujala, R.; Kauppinen, E. *J. Phys. Chem. C* **2012**, *116*, 632−636.
(27) Kaukonen, M.; Krasheninnikov, A. V.; Kauppinen, E.; Nieminen, R. M. *ACS Catal.* **2012**, *3*, 159−165.
(28) Sha, Y.; Yu, T. H.; Merinov, B. V.; Shirvanian, P.; Goddard, W. A. *J. Phys. Chem. Lett.* **2011**, *2*, 572−576.